HHS Public Access

Author manuscript

IEEE Trans Biomed Eng. Author manuscript; available in PMC 2022 August 11.

Published in final edited form as:

IEEE Trans Biomed Eng. 2020 August ; 67(8): 2194–2205. doi:10.1109/TBME.2019.2957392.

A New Neural Mass Model Driven Method and Its Application in Early Epileptic Seizure Detection

Jiang-Ling Song,
Medical Big data Research Center, Northwest University

Department of Neurology, Massachusetts General Hospital.

Qiang Li,
Medical Big Data Research Center, Northwest University.

Bo Zhang,
Medical Big Data Research Center, Northwest University.

M. Brandon Westover,
Department of Neurology, Massachusetts General Hospital.

Rui Zhang
Medical Big Data Research Center, Northwest University, Xi'an 710127, China

Abstract

Objective: Despite numerous neural computational models proposed to explain physiological and pathological mechanisms of brain activity, a large gap remains between theory and application of the models. Building on the successful application of data-driven methods in epileptic seizure detection, we aim to build a bridge between data and models in this paper.

Methods: We first propose a novel model-driven seizure detection method based on dynamic features in epileptic EEGs, where the rationale for dynamic features in epileptic EEGs can be clarified in theory by characterizing the variation of parameters of the model. Then we apply the proposed D&F-model-driven method to the problem of early epileptic seizure detection, where the evolution of model parameters selected and optimized by the proposed method is measured and used to detect the starting point of the seizure.

Results: Numerical results on two open EEG databases demonstrate that our proposed method does a good job of early epileptic seizure detection. The average detection sensitivity, false positive rate and early detection period attain 100%, 0.1/h, and 7.1 s respectively.

Conclusion: This paper provides a strategy to characterize EEG signals using a NMM-related method and the model parameters optimized by real EEG may then serve as features in their own right for early seizure detection.

Significance: An useful attempt to early detect epileptic seizures by combining the neural mass model with data analysis.

(Corresponding author: Rui Zhang.) rzhang@nwu.edu.cn.

Keywords

Neural mass model; dynamic feature; epilepsy; Electroencephalogram (EEG); early epileptic seizure detection

I. Introduction

Epilepsy is one of the most common neurological diseases, and disrupts the normal neuro-biologic, cognitive and psychological conditions of patients. Epilepsy is a condition of recurrent, unprovoked seizures, arising from abnormal excessive or hyper-synchronous neuronal activity in the brain [13]. Electroencephalography (EEG) is the primary method to record electrical activity generated by the brain, and is central to the diagnosis of epilepsy. However, visual inspection of long-term EEGs for detecting epilepsy is a time consuming and subjective process. Therefore, how to automatically analyze epileptic EEGs based on signal processing and machine learning methods is an active area of research.

Various automatic seizure detection methods from different points of view have been developed since the first work proposed in the 1970s [51]. In general, it is modeled as a binary classification problem, in which two states (seizure and non-seizure) are considered. In the cases where EEG signals are assumed to be stationary or pseudo-stationary, different features in the time domain (e.g., half-waves [51], linear prediction error energy (LPEE) [36], cross-correlation [39]) or frequency domain (e.g., power spectral density (PSD) [3]), combining with various classifiers (e.g., support vector machine (SVM) [24], [37], [39], [44], artificial neural networks (ANN) [5], [22], [27], [41], [47], [48] etc.), were proposed respectively to complete seizure detection. With the recognition of the non-stationary nature of EEG signals, the time-frequency analysis has been further investigated. The key idea is to apply different decomposition methods, including the continuous wavelet transform (CWT) [44], empirical wavelet transform [4], the local mean decomposition (LMD) [40] etc., to re-express the EEG signals, and then discriminate the seizure and non-seizure EEG signals. With the recognition that human brain activity can be regarded as a nonlinear dynamic process [23], various dynamic features have been explored to characterize epileptic events, such as complexity [28], [35], [45], [49], synchronization [17], [19], [25], persistence [47]. However, on one hand, such extracted epileptic EEG features are mostly heuristic, and hence, it is hard to give an explanation why these features work well in epileptic seizure detection. On the other hand, such data-driven seizure detection methods cannot give a detailed account of how the epileptic EEG evolves from the beginning of ictal evolution to the onset of disabling symptoms, which attracts more interests in the clinical concern.

Computational models provide a potential way to gain mechanistic insights into brain activity and the pathogenesis of brain disorders. A large number of computational models have been proposed in recent years, which can be divided into two classes: microscopic models and macroscopic models [16]. Microscopic models consider a large number of interconnected neurons, each represented by an explicit and detailed neuron model (e.g., Hodgkin-Huxley) [7], [11]. Although these models are more biologically realistic, the large number of parameters involved often makes relating these models to the underlying

biology problematic. By contrast, macroscopic models describe several interconnected neural populations under the assumption that neurons in the same population share similar electrophysiological properties. Each population in the model is characterized by a small number of state variables, including a post-synaptic potential, soma membrane potential, firing rate, and synaptic transmission delay [50]. Neural mass models (NMMs), among the most widely used macroscopic models, originated from the concept of a neural population proposed by Beurle in the early 1950s [1]. The Lopes da Silva model, which targets explaining the generation of the α rhythm in the thalamus [2], as well as Wilson&Cowan model, which aims to explain synchronization of neural oscillations [42], are considered two classical NMMs by most researchers. Building on these pioneering modeling studies, a variety of NMMs were developed and improved by adding new neural populations or connections to account for more and more complex physiological and pathological phenomena [12], [14], [30]–[34], [50].

Despite the large number of NMMs proposed to explain the physiological or pathological mechanisms of brain activity, there still exists a large gap between theory and application of the models. Inspired by recent successful applications of data-driven methods in seizure detection, in this paper we aim to build a bridge between data and model. A novel D&F-model-driven method based on dynamic features in epileptic EEGs will be first proposed. Then the proposed method will be applied to enable early epileptic seizure detection, which aims to find a window of time between the beginning of ictal evolution and the onset of disabling symptoms. The principal parameters in the model will be selected and optimized according to the proposed method, and evolution of the obtained parameters will be measured from the data to mark the starting point of the seizure. Numerical experimental results in clinically obtained EEG recordings will be presented to verify the performance of the proposed method and its application in early epileptic seizure detection.

The paper is organized as follows. In Section II, a brief overview of the D&F model and dynamic features in epileptic EEGs is presented, then the D&F-model-driven method based on dynamic features is proposed. Section III verifies the performance of the proposed method and its applications in early epileptic seizure detection in two open EEG databases. Some concluding remarks are given in the last section.

II. Method

In this section, we will first describe the structure and mathematical formulation of the ‘David & Friston model’. Then D&F-model-driven method based on dynamic features in epileptic EEGs will be proposed.

A. David & Friston Model

With the recognition that neurons in a population (excitatory or inhibitory) will have different reactions even though they receive the same stimulus, David and Friston proposed a new model to characterize such phenomenon in 2003 [32]. For convenience, we refer to this model as “D&F” in what follows. D&F is an extension of the J&R model [12], where each population in J&R model is divided into N sub-populations deployed in parallel with different kinetics. Fig. 1 illustrates the topological structure of D & F model.

Three types of neuron populations are included in D&F model: a pyramidal neuron population (PY), a local excitatory interneuron population (E), and a local inhibitory interneuron population (I). In each sub-population the weighted sum of all sub-population outputs is regarded as its final output. Populations E and I send postsynaptic firing rate to population PY, and receive postsynaptic potentials (PSP) from population PY through an excitatory feedback loop.

The transformation of electrical activities in D&F is realized by two computational blocks. The first computational block transforms the firing rate into the postsynaptic potential, formulated as

$$v_{e/i}(t) = (h_{e/i} \otimes m_{e/i})(t) \tag{1}$$

where

$$\begin{aligned} h_e(t) &= Aate^{-at},\ t \geq 0, \\ h_i(t) &= Bbte^{-bt},\ t \geq 0. \end{aligned} \tag{2}$$

In (1), the postsynaptic potential $v_{e/i}(t)$ is obtained by convolution of the presynaptic firing rate $m_{e/i}(t)$ and the impulse response $h_{e/i}(t)$, which can be equivalently solved by a second-order differential equation of the form

$$\ddot{v}(t) = \Gamma\gamma m(t) - 2\gamma\dot{v}(t) - \gamma^2 v(t)\,. \tag{3}$$

Eqs. (2) define the impulse responses $h_{e/i}(t)$. Here, parameters A and B represent the maximum amplitudes of the excitatory and inhibitory PSP (EPSP and IPSP), and a and b are the lumped representations of different time constants respectively. Symbols e/i represent excitatory or inhibitory subpopulations, and $\otimes$ denotes the convolution operation. In (3), $\Gamma = \{A, B\}$ and $\boldsymbol{\gamma} = \{a, b\}$.

By contrast, the second computational block transforms the postsynaptic potential into the firing rate, given by

$$m_{e/i}(t) = S(v_{e/i}(t)) \tag{4}$$

where

$$S(v) = \frac{2e_0}{1 + e^{r(v_0 - v)}}\,. \tag{5}$$

In (4), the postsynaptic firing rate $m_{e/i}(t)$ is the output of sigmoid function $S(\cdot)$ on $v_{e/i}(t)$. In the expression of $S(\cdot)$ in (5), parameter e_0 denotes the maximum firing rate of a population, v_0 is the firing threshold that determines the excitability of a population, and r represents the steepness of the sigmoidal transformation.

The transmission of electrical activity in D & F is realized by two forward connectivity passes “E → PY, I → PY” and two backward connectivity loops “PY → E, PY → I” (see

Fig. 1). We denote by C_1, C_2, C_3,C_4 the corresponding connectivity constants in backward loops, which account for the total number of E/I synapses connecting with the axons or dendrites of PY.

With the above preliminaries, the mathematical formulation of D&F model can be expressed by Eqs. in (6).

$$\begin{aligned}
\ddot{v}^n_{PY}(t) &= A_{PY,n}a_{PY,n}S\left[\sum_{n=1}^{N} w^n(v^n_E(t)-v^n_I(t))\right] \\
&\quad -2a_{PY,n}\dot{v}^n_{PY}(t) - a^2_{PY,n}v^n_{PY}(t), \\
\ddot{v}^n_E(t) &= A_{E,n}a_{E,n}\left(p(t)+C_2S\left[C_1\sum_{n=1}^{N} w^n(v^n_E(t))\right]\right) \\
&\quad -2a_{E,n}\dot{v}^n_E(t) - a^2_{E,n}v^n_E(t), \\
\ddot{v}^n_I(t) &= B_{I,n}a_{I,n}C_4S\left[C_3\sum_{n=1}^{N} w^n(v^n_I(t)-v^n_I(t))\right] \\
&\quad -2a_{I,n}\dot{v}^n_I(t) - a^2_{I,n}v^n_I(t), \quad n=1,\ldots,N,
\end{aligned} \tag{6}$$

Here, weight w^n is applied to represent the contribution of the nth sub-population in the model with the condition that $w^n \in [0, 1]$ and $\sum_{n=1}^{N} w^n = 1$.

According to the parameter values given in most prior work, we summarize the nominal values of all parameters in D&F model in Table I. Denote by $\Theta = \{A_{j,n}, B_{j,n}, a_{j,n}, C_i, v_0, e_0, r : j = E, I, PY; i = 1, 2, 3, 4; n = 1, \ldots, N\}$ the set of parameters in D&F model.

B. D&F-Model-Driven Method Based on Dynamic Features

This subsection introduces the D & F-model-driven method based on dynamic features in epileptic EEGs, whose purpose is to relate dynamic features that empirically have value in characterizing epileptic events to the dynamics of mechanistic models, building a bridge between data and model. It is known that the parameters within neural mass model be explicitly related to neurological mechanisms or physiological processes (that are potentially unidentified) [18]. It implies that tracking the variation of model parameters may be a better way to further understand the evolution of epilepsy. However, NMMs often employ several to several tens of parameters. Some of parameters may have limited impact on model behavior, while others have large effects. Hence, selecting those parameters which have the most influence on model behavior is of great significance. We name such parameters “principle parameters”. In this part, we propose a novel approach to determine the principle parameter vector based on the dynamic features of a non-stationary EEG signal. In our proposed method, we define the “sensitivity” of a parameter, which is formulated by the correlation between “parameter variation” and “feature variation”. That is to say, we want to know whether the system output will change significantly as each parameter changes, and which parameters will affect the output most. Here, features are extracted from the model output, and the output is calculated given a set of parameters. Therefore, features

change in response to changes in model parameter values. In this way, correlation between parameter values and features can be applied to measure the contribution of each parameter to the model behavior. Then the principle parameter vector is tracked by minimizing an error function, where the values of principle parameters are variables to be tuned to fit the data and other parameter values are set to their nominal values.

The key ideas of the D & F-model-driven method are summarized as follows. Denote by Θ the parameter vector of the model. We first select the principle elements from Θ which vary with the dynamic feature(s) of interest by analyzing which the relationship between the dynamic features extracted from the output signal of D&F and the corresponding parameters. Denote by $\bar{\Theta}$ the principle parameter vector. Then we find the optimal values in $\bar{\Theta}$ by minimizing an error function, which measures the difference between the epileptic EEG and the signals from the simulated D&F-model. We use $\bar{\Theta}^*$ to denote the optimal parameter vector. By solving this optimization problem we can explain the relationship between model and data, and hence, provide strong hypotheses for why various dynamic features work well in real applications.

Given a parameter vector $\Theta = (\theta_1, \theta_2, \ldots, \theta_m)$ and an individual increment $\Delta\theta_i$, we write

$$\Delta_i\Theta = (0, \ldots, \Delta\theta_i, \ldots, 0).$$

Then the outputs of D&F-model in terms of Θ and $(\Theta + \Delta_i\Theta)$ can be calculated by Eq. (6), denoted by $v(\Theta)$ and $v(\Theta + \Delta_i\Theta)$ respectively. Furthermore, we can extract features from $v(\Theta)$ and $v(\Theta + \Delta_i\Theta)$, which are denoted by $\mathbf{F}(v(\Theta))$ and $\mathbf{F}(v(0 + \Delta_i\Theta))$, provided that $\mathbf{F}$ is a one-dimensional dynamic feature. Writing

$$\Delta_i\mathbf{F}(\Theta) = \mathbf{F}(v(\Theta + \Delta_i\Theta)) - \mathbf{F}(v(\Theta)),$$

then for each element $\theta_i \in \Theta$, as increment $\Delta\theta_i$ changes, we define the sensitivity of θ_i as

$$Sen(\theta_i) = \frac{cov(\Delta\theta_i,\ \Delta_i\mathbf{F}(\Theta))}{\sqrt{Var(\Delta\theta_i)\ \cdot\ Var(\Delta_i\mathbf{F}(\Theta))}}. \tag{7}$$

Therefore, given a selection rule $\mathscr{R}$, the principle parameters can be defined as

$$\left\{\bar{\theta}_i \in \Theta : \mathscr{R}\left(\left|Sen\left(\bar{\theta}_i\right)\right|\right)\right\}. \tag{8}$$

Suppose that s elements in Θ are selected, we write the the vector of selected parameters as

$$\bar{\Theta} = \left(\bar{\theta}_1,\ \bar{\theta}_2, \ldots, \bar{\theta}_s,\ C(\theta_{s+1}), \ldots, C(\theta_m)\right). \tag{9}$$

where those non-selected parameters are set to their nominal values, denoted by $C(\theta_{s+1}), \ldots, C(\theta_m)$.

Next, we find the optimal values in $\bar{\Theta}$ by minimizing an error function. Given an EEG signal S, we first calculate the output $v(\bar{\Theta})$ of D&F where $v(\bar{\Theta})$ has the same number of samples

as S. For convenience in extracting features, we segment the signal into a sequence of K segments using sliding windows. Denote by

$$\mathbf{F}(S) = \left(\mathbf{F}_1^S,\ P_2^S, \ldots, \mathbf{F}_K^S\right)$$

and

$$\mathbf{F}(\upsilon(\overline{\Theta})) = \left(\mathbf{F}_1^\upsilon,\ \mathbf{F}_2^\upsilon, \ldots, \mathbf{F}_K^\upsilon\right).$$

the dynamic sequence of feature vectors. We then represent the histograms of $\mathbf{F}(S)$ and $\mathbf{F}(\upsilon(\overline{\Theta}))$ with the same number M of bins and the same size for each bin, denoted by $\mathbf{H}(S)$ and $\mathbf{H}(\upsilon(\overline{\Theta}))$. We compute the probability of each bin in $\mathbf{H}(S)$ and $\mathbf{H}(\upsilon(\overline{\Theta}))$ respectively, and write the corresponding vectors as

$$\mathbf{P}(S) = \left(P_1^S,\ P_2^S, \ldots, P_M^S\right) \tag{10}$$

and

$$\mathbf{P}(\upsilon) = \left(P_1^\upsilon,\ P_2^\upsilon, \ldots, P_M^\upsilon\right). \tag{11}$$

With the proceeding preliminaries, the error function is formulated by

$$E(\overline{\Theta}) = \sum_{m=1}^{M} \left(P_m^S - P_m^\upsilon\right)^2. \tag{12}$$

The optimal parameter vector is the solution to the optimization problem

$$\overline{\Theta}^* = \arg\min E(\overline{\Theta}). \tag{13}$$

Our D&F-model-driven optimization method is illustrated in Fig. 2, and the following algorithm formalizes the method.

Algorithm I (D&F-model-driven method): Given an EEG signal S, a dynamic feature extraction method $\mathbf{F}$ and D&F-model (Eqs. (6)).

Step 1: Determine the principle parameter vector $\overline{\boldsymbol{\Theta}}$.

for $i = 1 : m$,

1.1) generate the initial values of parameter vector Θ and incremental vector $\Delta_I\Theta$;

1.2) calculate the output of D&F-model in terms of Θ and $(\Theta + \Delta_I\Theta)$ according to Eq. (6);

1.3) compute dynamic features $\mathbf{F}(\Theta)$ and $\mathbf{F}(\Theta + \Delta_I\Theta)$;

1.4) calculate the sensitivities $Sen(\theta_i)$ for each i ($i = 1, \ldots, m$) according to Eq. (7).

end

The principle parameter vector $\overline{\boldsymbol{\Theta}}$ is determined according to Eqs. (8)–(9).

Step 2: Find the optimal parameter vector $\overline{\Theta}^*$.

2.1) calculate the output $\upsilon(\overline{\Theta})$;

2.2) compute dynamic features $\mathbf{F}(S)$ and $\mathbf{F}(\overline{\Theta})$;

2.3) formulate the error function $E(\overline{\Theta})$ according to Eqs. (10)–(12);

2.4) solve the optimization problem (13) and find the optimal solution $\overline{\Theta}^*$.

III. Application of the Proposed Method in Early Epileptic Seizure Detection

Different from seizure detection or prediction, early seizure detection aims to find the potential window of time between the beginning of ictal evolution and the onset of disabling symptoms, in which changes of brain electrical activity are measurable. As this period lasts only a few seconds in many cases, early seizure prediction is challenging. In this section, we apply the proposed method to early detection of epileptic seizures, a task which combines the model-driven and data-driven approaches to seizure analysis.

In the following, we first introduce two open EEG databases, the Bonn database and the CHB-MIT database. Then sample entropy, which characterizes signal complexity, will be summarized. Finally, we illustrate our approach by relating sample entropy to D&F model parameters in these EEG data sets.

A. Databases

The ***Bonn database*** is maintained by the Department of Epileptology, University of Bonn, and includes five datasets (denoted by Z, O, N, F and S). Each dataset consists of 100 single-channel scalp and intracranial EEGs with sampling rate 173.61 Hz and 12-bit A-D resolution. These EEGs are selected to be clear of artifacts. Details of the Bonn database are summarized in Table II.

CHB-MIT database is collected from 22 pediatric patients (5 males, ages 3–22; and 17 females, ages 1.5–19) with intractable seizures, who were monitored for up to several days following withdrawal of anti-seizure medication in Boston Children's Hospital. Most files contain 23-channel EEGs with sampling rate 256 Hz and 16-bit resolution. These include 198 seizures and the corresponding onset and offset times annotated by experts. Fig. 3 illustrates an EEG segment from recording "Chb01". Details of the database can be found in [6].

B. Model Selection

In our work, we apply a simple version of D&F model where $N = 2$. Accordingly, the mathematical expression of this model can be formulated by (14) (see page 7); all parameters are listed in Table III. Therefore, the model output can be calculated by

$$v(\Theta) = w(v_2 - v_3) + (1 - w)(v_6 - v_4).$$

Here, parameter vector

$$\Theta = (A,\ a,\ B,\ b,\ A,'\ a,'\ B,'\ b,\ e_0,\ r,\ v_0,\ C,\ w).$$

is a 13-dimensional vector where C_1, C_2, C_3, C_4 are multiples of C shown in Table I.

$$\begin{aligned}
\ddot{v}_1(t) &= AaS[wv_2(t) + (1-w)v_6(t) - wv_3(t) \\
&\quad -(1-w)v_4(t)] - 2a\dot{v}_1(t) - a^2 v_1(t) \\
\ddot{v}_2(t) &= Aa[p(t) - C_2 S[C_1(wv_1(t) + (1-w)v_5(t))]] \\
&\quad - 2a\dot{v}_2(t) - a^2 v_2(t) \\
\ddot{v}_3(t) &= BbC_4 S[C_3(wv_1(t) + (1-w)v_5(t))] \\
&\quad - 2b\dot{v}_3(t) - b^2 v_3(t) \\
\ddot{v}_4(t) &= B'b'C_4 S[C_3(wv_1(t) + (1-w)v_5(t))] \\
&\quad - 2b'\dot{v}_4(t) - b'^2 v_4(t) \\
\ddot{v}_5(t) &= A'a'S[wv_2(t) + (1-w)v_6(t) - wv_3(t) \\
&\quad -(1-w)v_4(t)] - 2a'\dot{v}_5(t) - a'^2 v_5(t) \\
\ddot{v}_6(t) &= A'a'[p(t) - C_2 S[C_1(wv_1(t) + (1-w)v_5(t))]] \\
&\quad - 2a'\dot{v}_6(t) - a'^2 v_6(t)
\end{aligned} \tag{14}$$

Fig. 4 illustrates the model outputs of the J&R model and D&F model with different parameter settings, respectively. As stated above, D&F is an extension of J&R; the general structures are identical (i.e., including three populations E,I and PY with same connectivity), but sub-populations were added in each population in D&F model. We can see from Fig. 4, compared with the outputs of J&R model (Fig. 4(a) and (b)), there is more clear spike-like morphology in the wave of Fig. 4(c). Besides, the slow rhythmic activity could be simulated by D&F model with a different weight parameter w (Fig. 4(d)). Such differences highlight the importance of sub-populations for modeling the diversity discharges, including epileptic activity.

C. Performance Verification of D&F-Model-Driven Method

In this subsection, performance of the D&F-model-driven method and its application in early epileptic seizure detection will be investigated in three ways: 1) determination of principle parameter vector; 2) determination of optimal parameter vector; 3) evaluation of performance in early epileptic seizure detection.

1) Determination of Principle Parameter Vector: Denoting $\Theta = \{\theta_i\}_{i=1}^{13}$, we first initialize parameter values and select increments based on uniform distributions, that is, $\theta_i \sim U[c_i, d_i]$ and $\Delta\theta_i \sim U[c_i * r, d_i * r]$. Here, the pairs (c_i, d_i) are determined based on nominal

values used in most references (Table VI) and $r = 0.1$. We randomly select 100 groups of Θ and $\Delta\theta_i$, and take sample entropy as a dynamic feature of interest **F**. The sensitivities of all parameters can then be calculated by Eq. (7). The obtained results are shown in Table IV. In our simulation, the principle parameter vector $\overline{\Theta}$ is determined by defining the energy ratio of sensitivity (ERS) of θ_i:

$$R_i = (NS_i)^2 / \max(NS_i)^2 . \tag{15}$$

In (15), NS_i denotes the normalized sensitivity of θ_i, which is computed by

$$NS_i = \frac{|Sen(\theta_i)| - \min_i\{|Sen(\theta_i)|\}}{\max_i\{|Sen(\theta_i)|\} - \min_i\{|Sen(\theta_i)|\}} .$$

Here ERS is a measure to characterize the contribution of each parameter. Then we take 75th percentile of all R_i as the baseline to select the "principle parameters". It could not only choose the parameters with more contributions, but also avoid the un-identifiability of the system caused by the redundancy of "principle parameters". According to the above procedure, the final obtained principle parameter vector is represented by

$$\overline{\Theta} = \{A,\ B,\ A,'\ B'\} .$$

According to our proposed method, the principle parameter vector is determined on the basis of sample entropy. It shows that parameters (A, B, $A,'$ B') in $\overline{\Theta}$ have more impact on the system's complexity than others. Fig. 5 illustrates the effect of A and B on sample entropy of the model output (similar results are obtained for the case of A' and B'). Seen from Fig. 5, as A increases and B decreases simultaneously, the sample entropy becomes smaller and smaller, which shows that lower and lower complexity of EEG signals is attained. Because $A(orA')$ and $B(orB')$ determine the maximum amplitude of the excitatory and inhibitory PSP [15], this observation is consistent with discoveries explaining the pathogenesis of at least some types of epileptic seizures [18]. Therefore, this result helps provide a mechanistic explanation for why entropy is a feature that works well in epileptic seizure detection.

2) Determination of Optimal Parameter Vector: In our work, we use an optimization approach based on a random walk, combined with a grid search (GS-RWO), to identify the optimal parameter vector $\overline{\boldsymbol{\Theta}}^*$.

First, we partition the parameter space $A \times B$ into a number of grids with identical side length 0.25 in the range [0,30] for A and [20,50] for B. We next calculate the error at each grid point (Ai, B_j)($i = 1, \ldots, 120$; $j = 1, \ldots, 120$) and select the one with minimum error, denoted $P_0 = (A_0, B_0)$. Then P_0 is considered to be the initial value of the random walk-based optimization method.

Second, given a neighborhood $U(P_0, \epsilon)$ (i.e. the initial walking step is ϵ), we randomly select one point $P' \in U(P_0, \epsilon)$ and compare the errors between them. If $E(P') \leq E(P_0)$, then the next walking point is updated to P', otherwise we keep P_0. The proceeding step is repeated until the terminating condition is satisfied. The values corresponding to the final obtained

point are the optimal parameter values we seek, A^* and B^*. Note that the optimal values of parameters A' and B' can be obtained in the same way. We write the optimal parameter vector as

$$\overline{\Theta}^* = \{A^*,\ B^*,\ (A')^*,\ (B')^*\}.$$

In the following, the performance of GS-RWO is demonstrated by taking A' as an example. We first generate a sequence of A' values which varies sinusoidally in [0,20] (see blue curve in Fig. 7(a)), which can taken as the "ground truth". With the generated sequence of A' and nominal values of other parameters, a sequence of the model output can be calculated by solving Eqs. (6). The obtained output sequence is regarded as an artificial EEG signal for this test. We next apply our D&F-model-driven method to the artificial EEG signal to obtain the optimal value of A' (red curve in Fig. 7(a)). Fig. 7(b) shows an example of simulated EEG with ground truth of parameter value A' = 7.9 (marked by the blue star in Fig. 7(a)). The obtained optimal value of A' is 8.5 (marked by the red star in Fig. 7(a)), and its corresponding model output is illustrated in Fig. 7(c). As seen in Fig. 7, simulated underlying values and the values obtained by the optimization procedure for A' match closely, demonstrating the effectiveness of the optimization approach.

We next focus on the relation between model parameters and entropy of real EEG signals. The parameters A, B are also taken as variables with others are set to be their nominal values. In this simulation, we first select 48 EEG segments (24 pre-ictal EEG segments and 24 ictal EEG segments) from 8 patents (each of them is 4 s). Then the corresponding sample-entropy-based frequency histogram (SE-FH) and the optimal values of parameters (A, B) are estimated for each EEG segment according to the proposed D&F-model-driven method with GS-RWO. Fig. 7 shows the effect of (A, B) on the sample entropy of the real EEGs. In Fig. 7(a), 48 points are marked whose position corresponds to the optimized parameters and whose value is the mean of its sample entropy in SE-FH. Fig. 7(b) and (c) illustrate two EEG segments as well as their SE-FHs, which corresponds to two points in Fig. 7(a) (marked by the blue and red dashed boxes). We can observe from Fig. 7 that most of the pre-ictal EEG segments are located at the upper-left of the graph having comparatively large values of sample entropy (corresponding to small A and large B), and most of ictal-EEG segments are located at the bottom-right of the graph having comparatively small values sample entropies (corresponding to small B and large A). Although a little overlaps exist between them, there still shows a relatively clear trend. That is, more and more ictal EEGs appear as A increases and B decreases simultaneously, which corresponds to the increasing excitation and decreasing inhibition of neural system. As a result, the generated imbalance between excitation and inhibition is consistent with one of the mechanisms to cause seizures [18].

3) Performance Verification on Early Epileptic Seizure Detection: Here we first show the effectiveness of the "principal model parameters" in differentiating seizure and non-seizure on Bonn database. Thirty EEG signals are randomly selected from data set F (inter-ictal EEGs) and set S (ictal EEGs) respectively. A 1 s sliding window was used to divide each EEG signal into segments. By applying the D&F-model-driven method on the

selected EEGs, we obtain the corresponding optimal parameter vectors, denoted $\overline{\Theta}_F^*$ and $\overline{\Theta}_S^*$ respectively. Fig. 8 illustrates four box plots of A_f, B_f (in $\overline{\Theta}_F^*$) as well as A_S, B_S (in $\overline{\Theta}_S^*$). It can be clearly seen that both the excitatory parameter A and the inhibitory parameter B are able to differentiate interictal and ictal EEG periods.

In the following, performance of the proposed method for early epileptic seizure detection is shown on CHB-MIT database. We select 8 patients whose seizure onset channels have been labelled [26]. The seizure onset channel, seizures, onset times and length of each seizure are listed in Table V.

As mentioned above, early seizure detection aims to find a window of time between the very beginning of ictal evolution and the onset of disabling symptoms. Therefore, whether such a time window can be detected via changes in model parameters, and if so how to mark the onset of the change, are the key points in model verification. We name the starting point found in this paper as the “seizure alarm time” in Table V.

We use a 4 s sliding window with 3 s overlaps to divide EEG signals into segments in the CHB-MIT database. For each EEG segment we calculate its sample-entropy-based frequency histogram, and evaluate the optimal model parameters. Fig. 9 illustrates the corresponding results of a 40s-long EEG signal, which includes 20 s pre-onset EEG followed by 20 s ictal EEG from “patient 1”. We can observe from Fig. 9 that the model parameters appear a clear variation trend from pre-onset to ictal, which shows that they are available for the early seizure detection. Specifically, model parameters $A(A')$ increases and $B(B')$ decreases suddenly almost at the same time around 2993 s, and 5 s later, the difference between A and B becomes much smaller. Based on such observation, we define an index

$$I(A,\ B) = \frac{(A\ -\ B)^2}{B}, \tag{16}$$

to measure the difference between A and B.

In simulations, we select one EEG file without any seizure for each patient, and decompose it as segments by 4 s sliding window without any overlap. After that, the non-consecutive 200 s segments without single spikes or other epileptiform waves are artificially chosen and defined as the “normal EEG segments” for each patient. Then the threshold λ is defined as the mean values of index (calculated by Eq. (16)) of all normal EEG segments. For a sequence of K EEG segments, we denote by $\{(A_k,\ B_k)\}_{k=1}^{K}$ the sequence of optimal parameter vectors and by $\{I_k = I(A_k,\ B_k)\}_{k=1}^{K}$ the sequence of indices of these values. The starting point of seizure is thus determined by

$$SP = \min_{3 \le k \le K} \{k : I_{k-2} \le \lambda,\ I_{k-1} \le \lambda,\ I_k \le \lambda\}.$$

Fig. 9(c) shows the starting point we find according to the above procedure, that is, $SP =$ 2984 s. By comparing with the starting point 2993 s shown in Fig. 9(b) which is observed

visually, this quantitatively marked starting point appears to be more reasonable and could be effective in early seizure detection.

The seizure alarm time (i.e., the starting point) and the early detected period for each seizure by our proposed method are shown in Table V. It can be seen that all of the detected alarm times are prior to the corresponding labelled onset times, where 11 out of 16 early detected period are greater than 6 s. These results verify the good performance of our proposed method. Furthermore, Figures 10(a)–(c) illustrate the results corresponding to “patient 2, 3 and 5”. Figures 10(a)–(c)(a) show three EEG segments including 20 s pre-onset EEG followed by ictal EEG with different length (9 s, 20 s, 20 s) from three patients respectively. Seizure onset time is marked for each segment as it is labelled in [26]; Figures 10(a)–(c)(b) show the detected alarm time and detected early seizure onset period for each EEG segment. All the results show good performance of D&F-driven-model method in early epileptic seizure detection.

IV. Discussion

In the present study, we have proposed a strategy to characterize EEG signals using a NMM-related method, which relies on optimizing principle parameters of the model in order to reduce error between dynamic features calculated from model output and EEG signal. Then the optimized parameters themselves serve as features in their own right for signal interpretation and early epileptic seizure detection.

We compare the performance between the proposed method with other existing methods. For the convenience of comparison, we have only listed those studies in which the seizure onsets scored by the algorithm and the expert are provided. The comparison results including the “detection sensitivity (%), detection FPR (/h) and detection period (s)” are shown in Table VI. Seen from Table VI, it can be concluded that: 1) the average detection sensitivity of the proposed technique is 100%, showing that all seizure are detected successfully; 2) the average FPR of the proposed technique is 0.1, showing that the times of false alarm is around 0.1 per hour; 3) the average detection period is 7.71 s, showing that the seizures onset could be detected 7.71 s earlier by the proposed technique than that labeled by expert. Comparing with other existing 7 techniques, we can observe that only two techniques have realized the early detection of seizures (that is, the work of Gardner [8] and our work). However, the omission ratio is 2.9% as well as the false alarm attains 1.56 times per hour in [8], which are much higher than ours. Here, we give the definitions of detection sensitivity, detection FPR [18] and detection period applied in this paper as follows.

$$Detection\ sensitivity = \frac{TP}{TP + FN},$$

$$Detection\ FPR = \frac{FP}{\text{Recording length}},$$

$$\textit{Detection period} = \text{mean value of early detected period of all seizures}.$$

The recording length and detailed results of FPR for 8 patients from CHB-MIT database are shown in last two columns of Table V.

To our best knowledge, few NMM-based works intended for seizure detection have been introduced in recent years. Although these approaches gained a certain level success in the application of NMMs for seizure detection, there still exists improvements to achieve better performances. In [29], Roessgen *et al.* firstly proposed a NMM-based seizure detection algorithm, which is based on a model adapted from Lopes da Silva *et al.* and applied to scalp EEG of two newborn babies. The authors included a seizure-generating component in a really simple NMM as a driver to seizure activities, to describe any physiological mechanisms for generating seizures. The model they used therefore assumed an outside epileptogenic driver to account for the general effect of various mechanisms, thus no hint about seizure generation can be derived [43]. In our work, we directly relate the parameters of a physiologically based model to neurological mechanisms. Aarabi *et al.* has proposed a model-based approach for hippocampal and neocortical early seizure detection [10]. Twelve model parameters, for each of the six contacts of each patient, were estimated by fitting the NMM to the power spectral. The method is quite complex, and the established patient-specific rules were difficult to interpret and were rather behavioral than relying on physiological assumptions [43]. Our method detects seizures upon the elevation of imbalance between excitation and inhibition (the corresponding parameters are selected by the proposed method), which is consistent with one of the mechanisms to cause seizures and has a straightforward interpretation. In 2013, Hocepied *et al.* employed a NMM based on the work of Jansen and Rit to complete the early detection of seizures [18]. However, it used a simpler model that did not allow simulation of more subtle neural behavior. Based on this, in 2019, an improved early seizure detection algorithm has been proposed [43]. It is based on automatic estimation of average synaptic gains by combining clinical data with a NMM according to the work of Wendling *et al.* However, the proposed algorithm has only been validated on intracranial electroencephalography (iEEG). In our work, a more complicated NMM, allowing to simulate various neural discharges including epileptiform activities, is applied. As well as, the proposed method is verified by employing the scalp EEG, which is the more complicated and widely used clinical signals compared with iEEG. In particular, although such two works were defined as “early seizure detection,” the evident detection delays existed in the presented results. Differently, the proposed method in our work indeed realizes to detect seizures 7.71 s seconds earlier than the labeled onset time in average.

Note that there are two reasons why dynamic features are applied to construct the error function between the model output and the real EEG signal in proposed method. On one hand, the D&F model in our work belongs to mesoscopic model, which applies the average activity of neuronal populations to represent the brain discharge in a local field. It is a typical over-simplified method to characterize the brain discharge. On the other hand, the EEGs applied in our work are recorded with the noninvasive electrodes placed along the scalp, where discharges of neuron assemblies are attenuated due to the existence of soft tissue and skull, as well as contaminated due to a significant presence of environmental noise and

artifacts. Under such situation, there must exist a big gap between the real EEG data and the model output themselves, so that it is difficult to apply the voltage difference between them to estimate the model parameter directly. Alternatively, we give more concern on epileptic features implied in EEGs rather than the waveform morphology (e.g., voltage).

Moreover, since sample entropy is a widely used dynamic features in seizure detection, we apply it in this work. However, we have to say that it is completely possible for other features being qualified to this work. Actually, the total power is also taken as a dynamic feature to construct the error function, and then verify the performance of the proposed method. Similar results can be obtained as shown in this work (due to the space limitation, the corresponding results are not shown here). From another point of view, it also cannot prove that all other dynamic features are effective for the proposed method to complete the early seizure detection. Hence, how to choose the appropriate features in the model-driven method will be a new direction in the future study.

Besides, the network-level features (such as synchronization and functional connectivity) are also important dynamic features of EEG. However, in order to incorporate these network-level features, the network-level neural computational models need to be constructed, which represent the interaction of multiple neural populations located in different cortical areas. Therefore, in the future study, the network-level neural computational modeling is a research frontier we are going to follow. It will not only be helpful to simulate EEGs more similar to the real EEGs, but also helpful to understand the network-level phenomenology in epilepsy, such as the synchronization between multiple channels, spreading of epileptiform waves, anterior-posterior lag or gradient. Network-level models may provide novel insight for understanding epilepsy and realizing early seizure detection more accurately.

Lastly, it should be noted that the proposed method has been verified only on 8 patients from open database (CHB-MIT), where the detail information of patients (such as the type of epilepsy) have not been published. But the seizure onset channel about each of them is known (as listed in Table V). We can see that seizure onset areas mainly locate temporal (right temporal: patients 1, 2; left temporal: patients 3, 4, 8, 10) and frontal (patients 5, 9) of cortex. It may imply that the proposed method has a good detection performance for temporal and frontal seizures. In the future work, it is important to cooperate with doctors and collect EEG signals in clinics with more detailed information, including the type of epilepsy, the location of epileptic focus etc. Then further study may be explored with such data, which is expected to find that the proposed method is effective for what kinds of epilepsy.

V. Conclusion

Herein we have proposed a novel D&F-driven-model method based on dynamic features in epileptic EEGs, which can be summarized via the following two steps: 1) the principle parameter vector is determined by analyzing the relationship between the dynamic features extracted from the output signal of D&F-model, using a novel “parameter sensitivity” measure; 2) the variable parameter vector is optimized by minimizing an error function, which is formulated according to the difference between the EEG and the signals simulated

via the D&F-model. We then applied the proposed D&F-driven-model method to early epileptic seizure detection. An index is defined to measure the evolution of the estimated model parameters and to detect the starting point of ictal evolution. Performance of our D&F-model-driven method and its applications are verified on two open EEG databases by evaluating three important aspects of the approach: 1) a procedure to select the principle parameter vector $\overline{\Theta}$ and its performance; 2) an optimization approach to obtain $\overline{\Theta}^*$ and its performance; 3) an index to mark the seizure starting point and its performance. Simulation results demonstrate that our proposed method does a good job in early epileptic seizure detection. The average detection sensitivity, false positive rate and early detection period attain 100%, 0.1/h, and 7.1 s respectively. It can be concluded that this paper provides a strategy to characterize EEG signals using a NMM-related method and the model parameters optimized by real EEG may then serve as features in their own right for early seizure detection, which is an useful attempt to early detect epileptic seizures by combining the neural mass model with data analysis.

Acknowledgments

This work was supported in part by the National Natural Science Foundation of China under Grant 61473223, in part by the Innovative Talents Promotion Plan of Shaanxi Province under Grant 2018TD-016, and in part by the Foundation for the National Institutes of Health of United States under Grants 1R01NS102190, 1R01NS102574, 1R01NS107291, 1RF1AG064312.

References

[1]. Beurle RL, “Poperties of a mass of cells capable of regenerating pulses,” Trans. Roy. Soc. (London) B, vol. 240, pp. 55–94, 1956.

[2]. Lopes Da Silva FH et al. , “Model of brain rhythmic activity,” Biol. Cybern, vol. 15, no. 1, pp. 27–37, 1974.

[3]. Subasi A et al. , “Comparison of subspace-based methods with AR parametric methods in epileptic seizure detection,” Comput. Biol. Med, vol. 36, pp. 195–208, 2006. [PubMed: 16389078]

[4]. Bhattacharyya A and Pachori RB, “A multivariate approach for patient-specific EEG seizure detection using empirical wavelet transform,” IEEE Trans. Biomed. Eng, vol. 64, no. 9, pp. 2003–2015, Sep. 2017. [PubMed: 28092514]

[5]. Naghsh-Nilchi AR et al. , “Epilepsy seizure detection using eigen-system spectral estimation and multiple layer perceptron neural network,” Biomed. Signal Process. Control, vol. 5, pp. 147–157, 2010.

[6]. Shoeb A et al. , “Patient-specific seizure onset detection,” Epilepsy Behav, vol. 5, no. 4, pp. 483–498, 2004. [PubMed: 15256184]

[7]. Hodgkin AL et al. , “The components of membrane conductance in the giant axon of loligo,” J. Physiol, vol. 116, no. 4, pp. 473–496, 1952. [PubMed: 14946714]

[8]. Gardner AB et al. , “One-class novelty detection for seizure analysis from intracranial EEG,” J. Mach. Learn. Res, vol. 7, pp. 1025–1044, 2006.

[9]. Aarabi A et al. , “A fuzzy rule-based system for epileptic seizure detection in intracranial EEG,” Clin. Neurophysiol, vol. 120, no. 9, pp. 1648–1657, 2009. [PubMed: 19632891]

[10]. Aarabi A et al. , “Seizure prediction in hippocampal and neocortical epilepsy using a model-based approach,” Clin. Neurophysiol, vol. 125, no. 5, pp. 930–940, 2014. [PubMed: 24374087]

[11]. Babajani-Feremi A et al. , “Multi-area neural mass modeling of EEG and MEG signals,” NeuroImage, vol. 52, pp. 793–811, 2010. [PubMed: 20080193]

[12]. Jansen BH et al. , “A neurophysiologically-based mathematical model of flash visual evoked potentials,” Biol. Cybern, vol. 68, pp. 275–283, 1993. [PubMed: 8452897]

[13]. Birjandtalab J et al. , “Automated seizure detection using limited-channel EEG and non-linear dimension reduction,” Comput. Biol. Med, vol. 82, pp. 49–58, 2017. [PubMed: 28161592]

[14]. Wendling F et al. , “Relevance of nonlinear lumped-parameter models in the analysis of depth-EEG epileptic signals,” Biol. Cybern, vol. 83, pp. 367–378, 2000. [PubMed: 11039701]

[15]. Wendling F et al. , “Epileptic fast activity can be explained by a model of impaired gabaergic dendritic inhibition,” Eur. J. Neurosci, vol. 15, pp. 1499–1508, 2002. [PubMed: 12028360]

[16]. Shayegh F et al. , “A brief survey of computational models of normal and epileptic eeg signals: A guideline to model-based seizure prediction,” J. Med. Signals Senors, vol. 1, pp. 70–79, 2011.

[17]. Mormann F et al. , “Mean phase coherence as a measure for phase synchronization and its application to the EEG of epilepsy patients,” Physica D, vol. 144, pp. 358–369, 2000.

[18]. Hocepied G et al. , “Early detection of epileptic seizures based on parameter identification of neural mass model,” Comput. Biol. Med, vol. 43, pp. 1773–1782, 2013. [PubMed: 24209923]

[19]. Yu H et al. , “Investigation of phase synchronization of interictal EEG in right temporal lobe epilepsy,” Physica A, Statistical Mechanics Appl, vol. 492, pp. 931–940, 2018.

[20]. Qu H et al. , “A seizure warning system for long-term epilepsy monitoring,” Neurol, vol. 45, no. 12, pp. 2250–2254, 1995.

[21]. Osorio I et al. , “Real-time automated detection and quantitative analysis of seizures and short-term prediction of clinical onset,” Epilepsia, vol. 39, no. 6, pp. 615–627, 1998. [PubMed: 9637604]

[22]. Song J et al. , “Automated detection of epileptic EEGs using a novel fusion feature and extreme learning machine,” Neurocomput, vol. 175, pp. 383–391, 2016.

[23]. Song J et al. , “Application of extreme learning machine to epileptic seizure detection based on lagged poincaŕe plots,” Multidimensional Syst. Signal Process, vol. 28, no. 3, pp. 945–959, 2017.

[24]. Joshi V et al. , “Classification of ictal and seizure-free EEG signals using fractional linear prediction,” Biomed. Signal Process. Control, vol. 9, pp. 1–5, 2014.

[25]. Majumdar K et al. , “Synchronization implies seizure or seizure implies synchronization?” Brain Topogr, vol. 27, no. 1, pp. 112–122, 2014. [PubMed: 23563905]

[26]. Chen L-L et al. , “A framework on wavelet-based nonlinear features and extreme learning machine for epileptic seizure detection,” Biomed. Signal Process. Control, vol. 10, pp. 1–10, 2014.

[27]. Guo L et al. , “Automatic epileptic seizure detection in EEGs based on line length feature and artificial neural network,” J. Neurosci. Methods, vol. 191, pp. 101–109, 2010. [PubMed: 20595035]

[28]. Tito M et al. , “Classification of electroencephalographic seizure recordings into ictal and interictal files using correlation sum,” Comput. Biol. Med, vol. 39, pp. 604–614, 2009. [PubMed: 19467652]

[29]. Roessgen M, Zoubir AM, and Boashash B, “Seizure detection of newborn eeg using a model-based approach,” IEEE Trans. Biomed. Eng, vol. 45, no. 6, pp. 673–685, Jun. 1998. [PubMed: 9609933]

[30]. Ursino M et al. , “The generation of rhythms within a cortical region: Analysis of a neural mass model,” NeuroImage, vol. 52, pp. 1080–1094, 2010. [PubMed: 20045071]

[31]. Moran R et al. , “A neural mass model of spectral responses in electrophysiology,” Neuroimage, vol. 37, pp. 706–720, 2007. [PubMed: 17632015]

[32]. David O et al. , “A neural mass model for MEG/EEG: Coupling and neuronal dynamics,” NeuroImage, vol. 20, pp. 1743–1755, 2003. [PubMed: 14642484]

[33]. David O et al. , “Modelling event-related responses in the brain,” NeuroImage, vol. 25, pp. 756–770, 2005. [PubMed: 15808977]

[34]. Wang P et al. , “A realistic neural mass model of the cortex with laminar-specific connections and synaptic plasticity evaluation with auditory habituation,” PLos One, vol. 8, pp. 1–17, 2013.

[35]. Yuan Q et al. , “Epileptic EEG classification based on extreme learning machine and nonlinear features,” Epilepsy Res, vol. 96, pp. 29–38, 2011. [PubMed: 21616643]

[36]. Altunay S et al. , “Epileptic EEG detection using the linear prediction error energy,” Expert Syst. Appl, vol. 37, pp. 5661–5665, 2010.

[37]. Li S et al. , “Feature extraction and recognition of ictal EEG using EMD and SVM,” Comput. Biol. Med, vol. 43, pp. 807–816, 2013. [PubMed: 23746721]

[38]. Grewal S et al. , “An automatic warning system for epileptic seizures recorded on intracerebral EEGs,” Clin. Neurophysiol, vol. 116, no. 10, pp. 2460–2472, 2005. [PubMed: 16125459]

[39]. Chandaka S et al. , “Cross-correlation aided support vector machine classifier for classification of EEG signals,” Expert Syst. Appl, vol. 36, pp. 1329–1336, 2009.

[40]. Zhang T and Chen W, “LMD based features for the automatic seizure detection of EEG signals using SVM,” IEEE Trans. Neural Syst. Rehabil. Eng, vol. 25, no. 8, pp. 1100–1108, Aug. 2017. [PubMed: 27662677]

[41]. Orhan U et al. , “EEG signals classification using the K-means clustering and a multilayer perceptron neural network model,” Expert Syst. Appl, vol. 38, pp. 13475–13481, 2011.

[42]. Wilson HR et al. , “Excitatory and inhibitory interactions in localized populations of model neurons,” Biophysical J, vol. 12, no. 1, pp. 1–24, 1972.

[43]. Fan X et al. , “Automated epileptic seizure detection based on break of excitation/inhibition balance,” Comput. Biol. Med, vol. 107, pp. 30–38, 2019. [PubMed: 30772528]

[44]. Li Y et al. , “Epileptic seizure detection based on time-frequency images of EEG signals using Gaussian mixture model and gray level co-occurrence matrix features,” Int. J. Neural Syst, vol. 28, no. 07, 2018, Art. no. 1850003.

[45]. Kumar Y et al. , “Epileptic seizure detection using DWT based fuzzy approximate entropy and support vector machine,” Neurocomput, vol. 133, pp. 271–279, 2014.

[46]. Zhang Y et al. , “An automatic patient-specific seizure onset detection method in intracranial EEG based on incremental nonlinear dimension-alityreduction,” Comput. Biol. Med, vol. 40, no. 11–12, pp. 889–899, 2010. [PubMed: 20951372]

[47]. Yuan Q et al. , “Epileptic EEG classification based on extreme learning machine and nonlinear features,” Epilepsy Res, vol. 96, no. 1, pp. 29–38, 2011. [PubMed: 21616643]

[48]. Song Y et al. , “A new approach for epileptic seizure detection: Sample entropy based feature extraction and extreme learning machine,” J. Biomed. Sci. Eng, vol. 3, no. 06, pp. 556–567, 2010.

[49]. Song Y et al. , “Automated epileptic seizure detection in EEGs based on optimized sample entropy and extreme learning machine,” J. Neurosci. Methods, vol. 210, pp. 132–146, 2012. [PubMed: 22824535]

[50]. Zavaglia M et al. , “A neural mass model for the simulation of cortical activity estimated from high resolution EEG during cognitive or motor tasks,” J. Neurosci. Methods, vol. 157, no. 2, pp. 317–329, 2006. [PubMed: 16757033]

[51]. Gotman J, “Automatic recognition of epileptic seizures in the EEG,” Electroencephalogr. Clin. Neurophysiol, vol. 54, no. 5, pp. 530–540, 1982. [PubMed: 6181976]

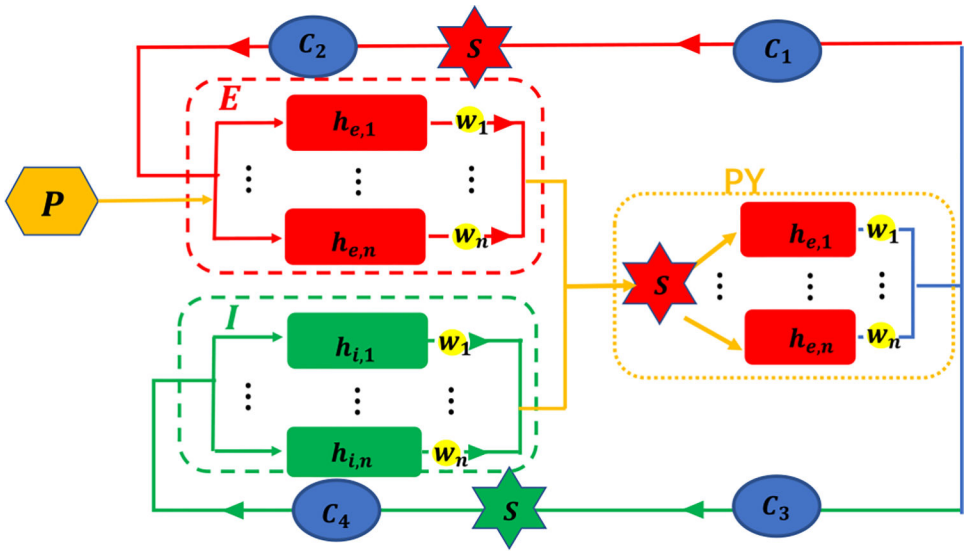

Fig. 1.
Schematic of the D&F model.

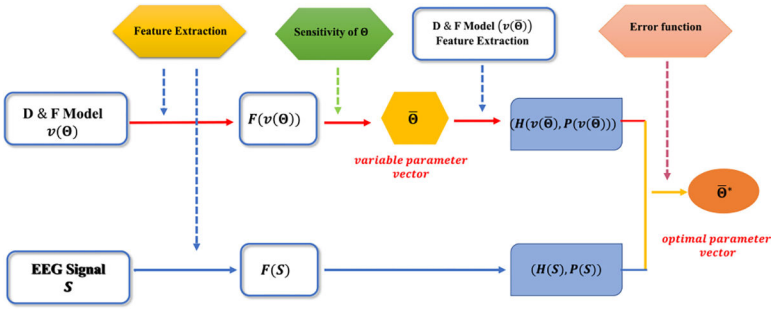

Fig. 2.
Optimizaton procedure for the D&F-model-driven method.

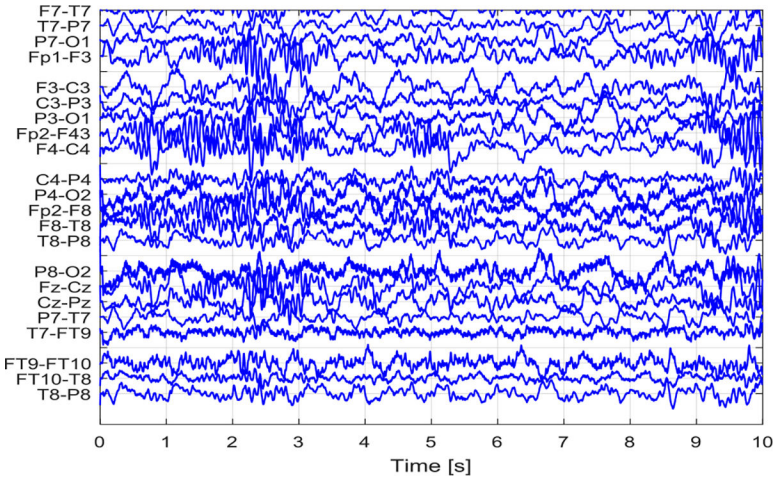

Fig. 3.
An EEG sample in CHB-MIT database.

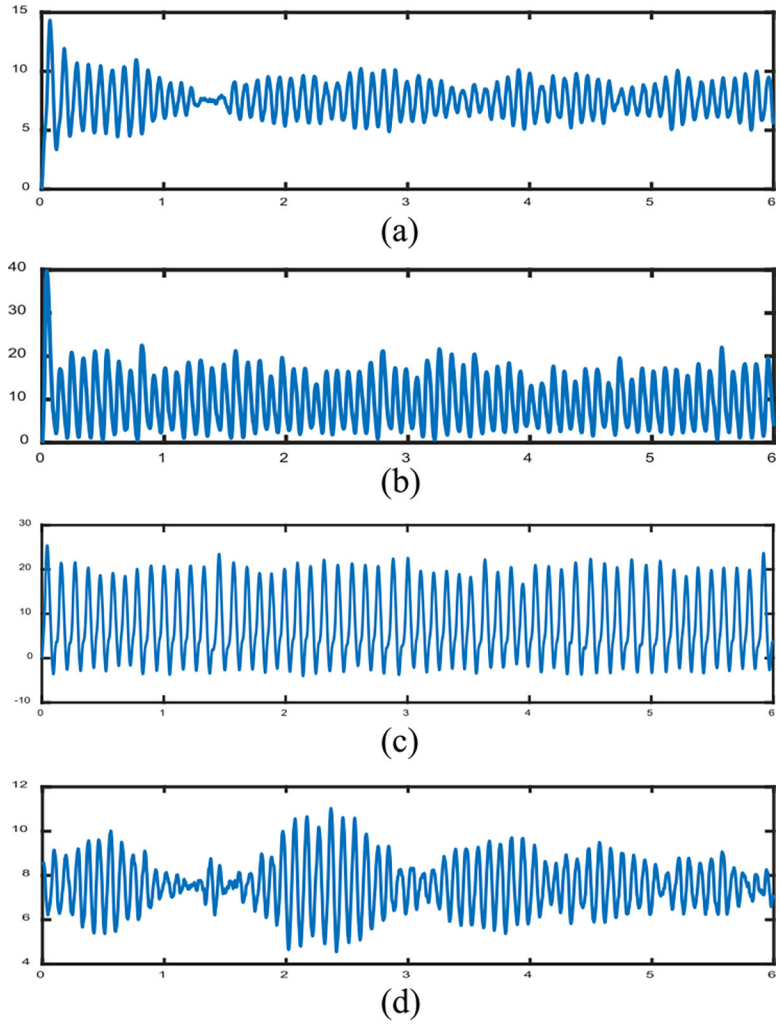

Fig. 4.

Model outputs of J&R model (without sub-population) and D&F model (with 2 sub-populations). (a) J&R model with parameter $A = 3.25$, $B = 22$. (b) J&R model with parameter $A = 5.25$, $B = 22$. (c) D&F model with parameter $A = 3.25$, $A' = 5.25$, $B = 22$, $B' = 22$, $w = 0.5$. (d) D&F model with parameter $A = 3.25$, $A' = 5.25$, $B = 22$, $B' = 22$, $w = 0.9$.

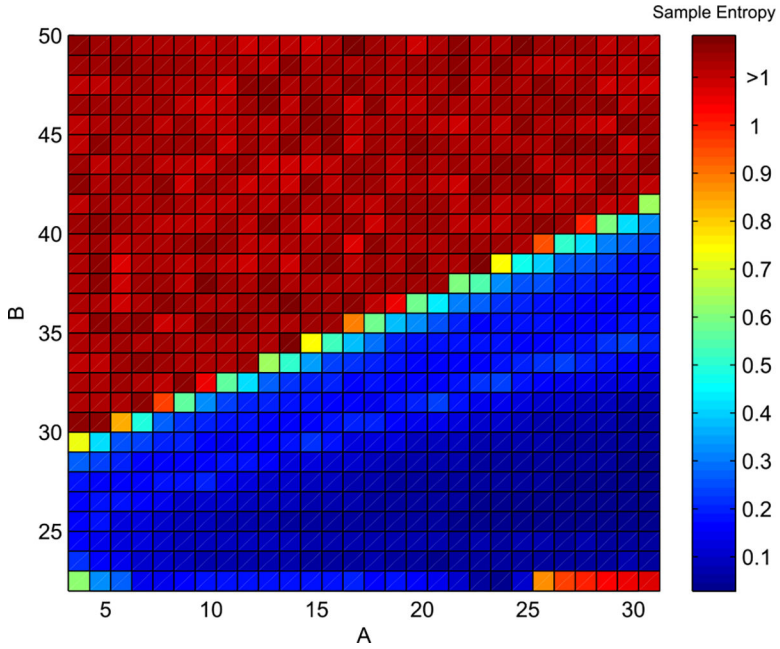

Fig. 5.
The effect of A, B on the sample entropy of the model output

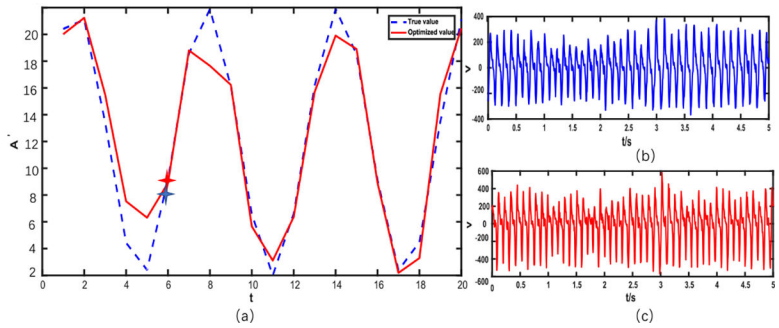

Fig. 6.

Comparison between true (simulated) values and the optimized values of A' obtained by GS-RWO.

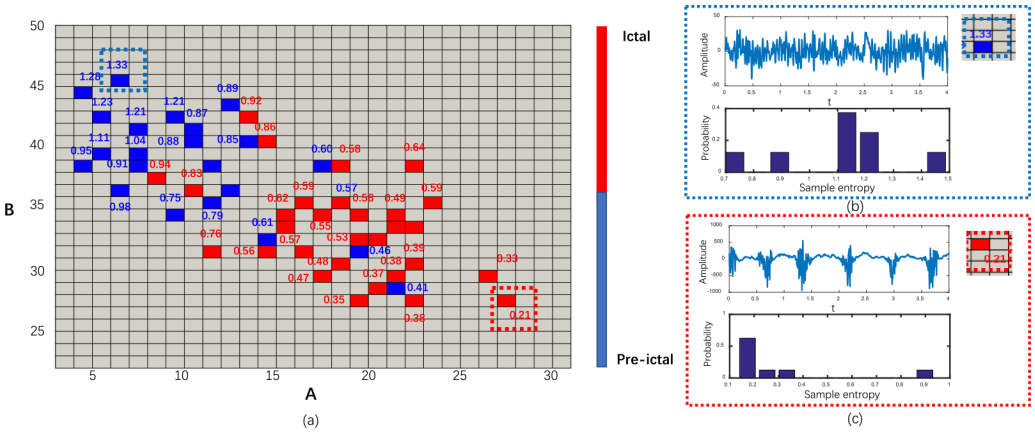

Fig. 7.
The effect of (A, B) on the sample entropy of the real EEGs.

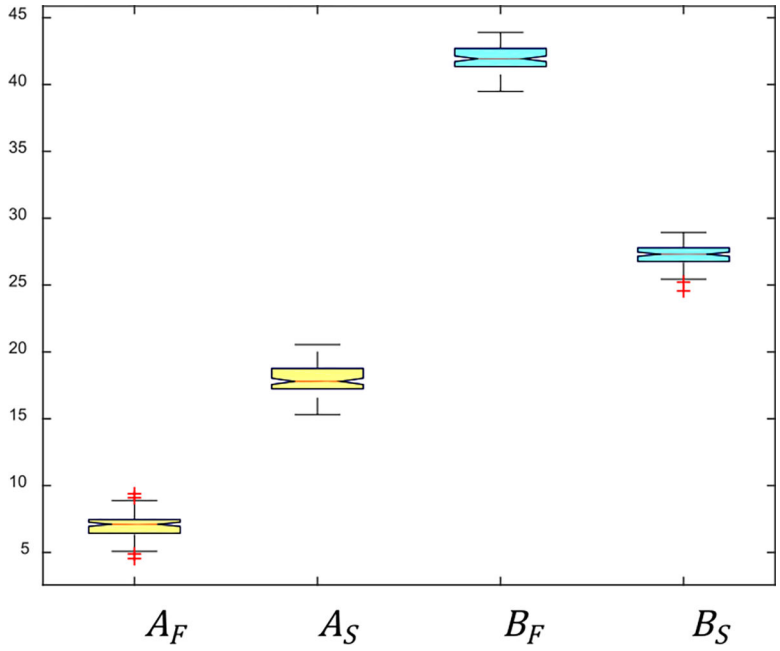

Fig. 8.

Box plots of the excitatory parameter A and the inhibitory parameter B on the Bonn database (F and S).

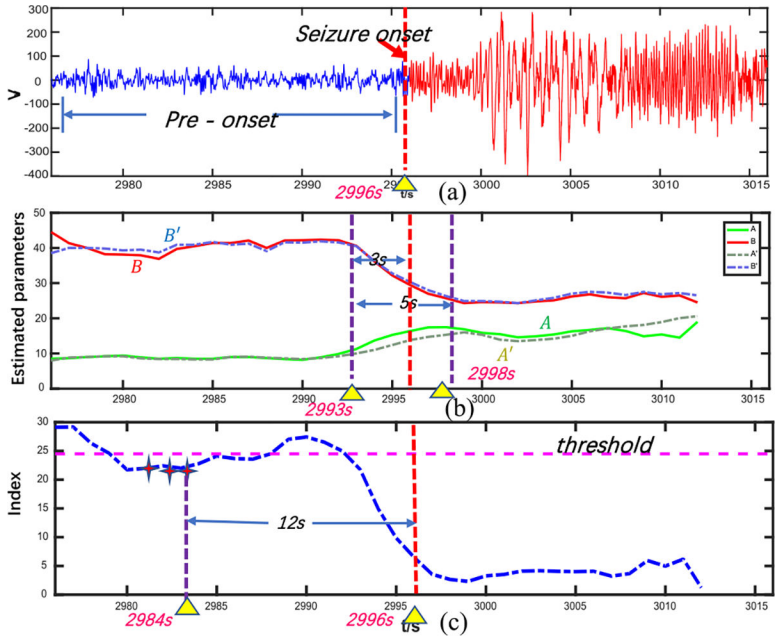

Fig. 9.

(a) A 40s-long EEG signal including 20 s pre-seizure-onset followed by 20 s of ictal EEG from “patient 1”; (b) The sequence of optimal parameters $A, A, {}'B', B';$ (c) The sequence of indices $I(A, B)$ with the early detected period.

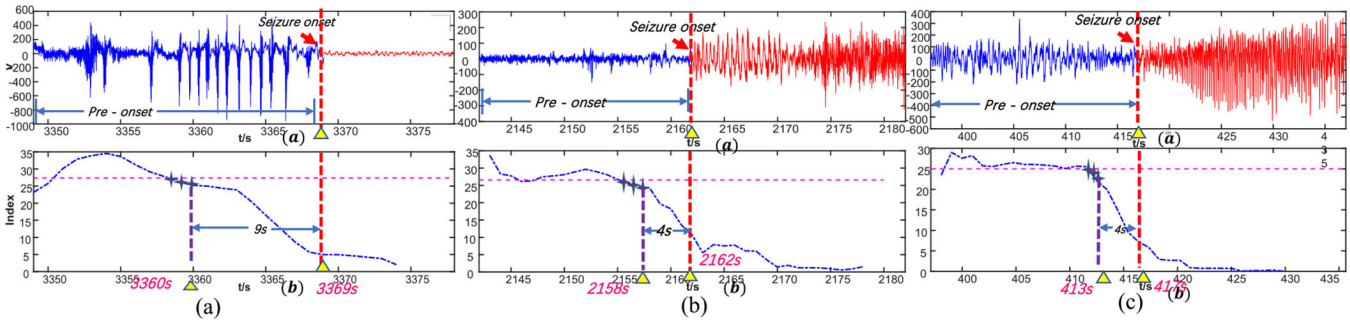

Fig. 10.

(a) a: A 29s-long EEG signal including 20 s pre-onset EEG followed by 9 s ictal EEG for “patient 2” and corresponding sequence of indexes with the early detected period. (b) a: A 40s-long EEG signal including 20 s pre-onset EEG followed by 20 s ictal EEG for “patient 3” and corresponding sequence of indexes with the early detected period. (c) a: A 40s-long EEG signal including 20 s pre-onset EEG followed by 20 s ictal EEG for “patient 5” and corresponding sequence of indexes with the early detected period.

TABLE I

Nominal Values of Parameters in D&F Model

Parameters	Nominal values
$A_{j,n}$, $B_{j,n}$	$A_{j,n} = 3.25mV$, $A_{j,n} = 22mV$
$a_{j,n}$, $b_{j,n}$	$a_{j,n} = 100$, $b_{j,n} = 50$
C_1, C_2, C_3, C_4	$C_1 = C$, $C_2 = 0.8C$, $C_3 = C_4 = 0.25C$, $C = 135$
v_0, e_0, r	$v_0 = 6mV$, $e_0 = 5s^{-1}$, $r = 0.56mV^{-1}$

TABLE II

Information Regarding the Bonn Seizure Database

Data set	recording electrodes	recorded position	subject state
Z	scalp	cortex	awake and relaxed state with eyes open of five healthy people
O	scalp	cortex	awake and relaxed state with eyes closed of five healthy people
N	intracranial	hippocampal	period of inter-ictal of epilepsy patients
F	intracranial	epileptogenic zone	period of inter-ictal of epilepsy patients
S	intracranial	epileptogenic zone	period of ictal of epilepsy patients

TABLE III

Parameters in D&F Model (N = 2)

	excitatory populations E, PY	**inhibitory population I**
sub-population 1	A, a	B, b
sub-population 2	A', a'	B', b'
sub-populations 1 and 2	e_0, r, v_0, w, C_1, C_2, C_3, C_4	

TABLE IV

Sensitivity of All Parameters

Parameter	Sensitivity	ERS	Parameter	Sensitivity	ERS
A	0.2413	49.87%	a'	0.0315	0.42%
B	−0.3377	100%	b'	−0.0322	0.45%
a	0.1076	8.83%	C	−0.1131	9.86%
b	−0.0782	4.3%	e_0	−0.0854	5.26%
A'	0.2481	52.76%	r	0.0103	0
B'	−0.2029	38.61%	v_0	0.0372	0.68%
w	−0.0393	0.78%			

TABLE V

Detailed EEG Information for 8 Patients and Early Detection Results

Patient	Channel	Seizures	Onset time	Seizure length	Alarming time	Early detected period	Recording length	FPR
		*chb*01$_{03}$	2996s	40s	2884s	12s		
		*chb*01$_{04}$	1467s	27s	1461s	6s		
		*chb*01$_{15}$	1732s	40s	1731s	1s		
patient 1	T8-P8	*chb*01$_{16}$	1015s	51s	1014s	1s	5hrs	0.2
		*chb*01$_{18}$	1720s	90s	1719	1s		
patient 2	T8-P8	*chb*02$_{16}$	2972s	81s	2963s	9s	2hrs	0
		*chb*02$_{19}$	3369s	9s	3360s	9s		
		*chb*03$_{01}$	362s	52s	352s	10s		
		*chb*03$_{02}$	731s	65s	720s	11s		
patient 3	T7-P7	*chb*03$_{03}$	432s	69s	420s	12s	5hrs	0
		*chb*03$_{04}$	2162	52s	2158s	4s		
		*chb*03$_{34}$	1982s	47s	1968s	14s		
patient 4	T7-P7	*chb*04$_{05}$	7804s	49s	7881s	3s	3hrs	0
		*chb*04$_{08}$	6446s	111s	6438s	8s		
		*chb*04$_{28}$	1679s	102s	1669s	10s		
patient 5	F7-T7	*chb*05$_{06}$	417s	115s	406s	11s	4hrs	0
		*chb*05$_{13}$	1086s	110s	1074s	12s		
		*chb*05$_{16}$	2317s	96s	2309s	8s		
		*chb*05$_{17}$	2451s	66s	2441s	10s		
patient 8	T7-P7	*chb*08$_{02}$	2670s	171s	2661s	9s	4hrs	0.25
		*chb*08$_{05}$	2856s	190s	2843s	13s		
		*chb*08$_{11}$	2988s	134s	2994 s	4s		
		*chb*08$_{13}$	2417s	160s	2406s	11s		

IEEE Trans Biomed Eng. Author manuscript; available in PMC 2022 August 11.

Patient	Channel	Seizures	Onset time	Seizure length	Alarming time	Early detected period	Recording length	FPR
patient 9	F7-T7	$chb09_{06}$	12231s	64s	12225s	6s	3hrs	0
		$chb09_{08}$	2051s	79s	2045s	6s		
		$chb09_{19}$	5299s	62s	5292s	7s		
patient 10	T7-P7	$chb10_{12}$	6313s	35s	6310s	3s	5hrs	0.4
		$chb10_{20}$	6888s	70s	6878s	10s		
		$chb10_{27}$	2382s	65s	2377s	7s		
		$chb10_{30}$	3021s	58s	3017s	4s		
		$chb10_{38}$	4618s	89s	4611s	7s		

TABLE VI

The Comparison Results Between the Proposed Method and Other Techniques

Authors	Sensitivity (%)	FPR (/h)	Detection period (s)
Qu and Gotman [20]	100	0.37	−9.6
Osrio et al. [21]	100	0	−2.1
Grewal and Gotman [38]	89.4	0.22	−17.1
Gardner et al. [8]	97.1	1.56	7.58
Aarabi et al. [9]	98.7	0.27	−11
Zhang et al. [46]	98.8	0.24	−10.8
Gatien Hocepied et al. [18]	96.0	0.14	−14.3
This paper	100	0.1	7.71